Available online at www.sciencedirect.com

ScienceDirect

Journal of the Franklin Institute 359 (2022) 6467–6485

www.elsevier.com/locate/jfranklin

Dixon resultant theory for stability analysis of distributed delay systems and enhancement of delay robustness

Qingbin Gao[a], Jiazhi Cai[a], Peyman Firoozy[b], Shenghui Guo[c], Hanlin Hong[d], Zhili Long[a,*]

[a] *School of Mechanical Engineering and Automation, Harbin Institute of Technology (Shenzhen), Shenzhen, China*
[b] *Department of Mechanical Engineering, Bilkent University, Ankara, Turkey*
[c] *School of Electronics and Information Engineering, Suzhou University of Science and Technology, Suzhou, China*
[d] *Wuji Technology Beijing Co., Ltd, Beijing, China*

Received 8 October 2021; received in revised form 17 March 2022; accepted 16 May 2022
Available online 1 June 2022

Abstract

This study scrutinizes the stability problem of linear time-invariant feedback control systems with a constant-coefficient, partial delay distribution from a new perspective, which is built on an equivalence between the system of interest and the one with two lumped delays. We aim to determine all the potential stability changing curves (PSCC) of the system in the domain of delays in order to make a non-conservative stability assessment. First, we propose the Dixon resultant-based frequency sweeping procedure to calculate the so-called kernel and offspring hypersurfaces (KOH) of the system. The superiority in the computational efficiency of this Dixon-type method is revealed by comparison with the Sylvester-type one. Second, we specifically tackle the standing root case for the singularity at the zero root, leading to what we call the standing root boundary (SRB). Then, we claim that the union of the KOH and SRB constitutes the PSCC of the system. With these, the stability map of the system is then created using the Cluster Treatment of Characteristic Roots paradigm. Furthermore, we declare the delay robustness is enhanced by the proposed control law. Finally, we demonstrate the effectiveness of the presented procedures over two example case studies by the Quasi-Polynomial mapping-based Root-finder routine as well as the Simulink-based simulation.

https://doi.org/10.1016/j.jfranklin.2022.05.034

1. Introduction

Time-delayed dynamics never fail to fascinate researchers in the control field over the past few decades. Among numerous publications, the systems with distributed-delayed feedback evince distinctive features by different distributed kernel functions to reflect the inherent memory effects, e.g., the uniform distribution [1–3], gamma distribution with or without gap [2,4], and constant-coefficient distribution [5,6]. Readers are also referred to the associated applications to the car-following system [2,3], input signal shaper [7], and active vibration suppression [8]. The distributed delay serves as a moving filter and enhances the delay robustness [3,9] as opposed to the lumped (or pointwise) delay. In this study, we uniquely consider the distributed-delayed feedback with a constant coefficient, partial distribution. Then, the biggest concern is the stability robustness against *large* delay uncertainties associated with this control logic. By 'large', we mean the delays under consideration are in the order of 1s, not 10^{-1}s or 10^{-2}s.

For the stability assessment of time-delay systems, both time-domain and frequency-domain strategies are frequently involved since each of them has strengths and limitations. The time-domain methodologies, which typically resort to Lyapunov functions or Lyapunov functionals, have wider applicability to various dynamics, e.g., time-varying delays [10] and delayed fuzzy systems [11]. By contrast, the frequency-domain approaches are famous for their exact and non-conservative results, c.f. [12–15]. An influential paradigm named the Cluster Treatment of Characteristic Roots (CTCR) [16–18] is presented to evaluate the stability of linear time-invariant (LTI) systems with constant delays in the entire domain of delays (a.k.a. the complete stability analysis). The CTCR paradigm entails all the potential stability changing curves (PSCC) in the delay space, which can be acquired by the frequency sweeping framework [14,19,20]. However, the computational cost is another serious concern given that the computing resources at hand are limited and the analysis is NP-hard [21].

Furthermore, the characteristic equation for the system with constant-coefficient delay distribution is ill-posed when the root is at zero, namely, a removable singular point would occur [6]. The treatment of this singularity is vital since it gives rise to some extra stability boundaries which are not revealed otherwise when delays vary. Very recently, a class of fractional-order systems with such constant-coefficient distributed delays is considered in [22]. However, we argue that the stability inspection in [22] is incomplete since the singularity is not considered.

In light of this, the main contributions of our work are threefold. First, the *Dixon resultant*-based frequency sweeping procedure [20,23] is developed to calculate the kernel and offspring hypersurfaces (KOH) for the system of interest. The computational advantages of this unique approach over the Sylvester resultant-based one [12] are then emphasized to improve the computational efficiency. Second, the standing root analysis is presented to handle the removable singularity, leading to what we call the standing root boundary (SRB). With these, the *complete stability map* is revealed by the CTCR paradigm using the PSCC, the union of the KOH and SRB. Last, we prove the proposed control law with distributed delays can greatly improve the delay robustness compared to the one with a single lumped delay.

* Corresponding author.
E-mail address: longzhili@hit.edu.cn (Z. Long).

The remainder of the text is organized as follows. Section 2 offers some preparatory knowledge of the system with distributed-delayed feedback. The main results of the stability assessment for the considered system are provided in Section 3. In Section 4, we demonstrate the strength of the proposed procedures over two example case studies. For the completeness of discussion, a brief overview of the CTCR paradigm is given in Appendix, which is borrowed from Ergenc et al. [17].

2. Preliminaries

Consider a general class of LTI distributed delay systems with a *constant-coefficient, partial delay distribution*:

$$\dot{\mathbf{x}}(t) = \mathbf{A}\mathbf{x}(t) + \mathbf{B}\int_{\tau_1}^{\tau_2} \mathbf{x}(t-\vartheta)d\vartheta \tag{1}$$

where $\mathbf{x}(t) = [x_1(t), x_2(t), \dots x_n(t)]^{\mathrm{T}} \in \mathbb{R}^n$ is the state vector, $\mathbf{A}, \mathbf{B} \in \mathbb{R}^{n\times n}$ are constant, known matrices, and $(\tau_1, \tau_2) \in \mathbb{R}^{2+}$ is the delay vector for the integral bounds of the distributed delay parameter $\vartheta \in \mathbb{R}^+$ so that $\tau_1 \le \vartheta \le \tau_2$. The following assumption is made to further clarify the proposed distributed control strategy in Eq. (1).

Assumption 1. Assume that all the states identically experience the *inherent delay* $\tau_1 > 0$ and what we call the *compensatory delay* $\tau_2 > \tau_1$, and $\mathbf{x}(t-\vartheta) = \mathbf{0}$ for $t - \vartheta < 0$.

Then, all the state information is available from the time instant 0 to $t - \tau_1$ under Assumption 1, signifying that τ_1 dictates the earliest delayed outputs that the controller can store. The *partial* state information from $t - \tau_2$ to $t - \tau_1$ is picked up to constitute the feedback input in Eq. (1) with *constant-coefficient* distributed delay. In this setting, τ_1 *inherently* exists owing to the computation and communication lags while τ_2 is artificially configured in the feedback line to *compensate* for the delay effects. The main objective is the determination of stability robustness against delay uncertainties. In other words, this study aims at evaluating the stability posture in the entire (τ_1, τ_2) space and seeking for the feasible τ_2 parameter that stabilizes the plant for a certain τ_1 value.

Remark 1. We also wish to mention the system with a single lumped delay for the comparative purpose:

$$\dot{\mathbf{x}}(t) = \mathbf{A}\mathbf{x}(t) + \mathbf{B}\mathbf{x}(t-\tau_1) \tag{2}$$

where τ_1 is the *inherent delay* and this dynamic model is referred to as the lumped control law. The comparison of the delay robustness between the control strategies in Eqs. (1) and (2) is made in Section 4.

Next, the following equation is obtained by taking the Laplace transform of Eq. (1):

$$s\mathbf{X}(s) = \mathbf{A}\mathbf{X}(s) + \mathbf{B}\int_{\tau_1}^{\tau_2} \mathbf{X}(s)e^{-\vartheta s}d\vartheta \tag{3}$$

where s is the Laplace variable and $\mathbf{X}(s) = \mathcal{L}\{\mathbf{x}(t)\}$. It is noteworthy that $\mathbf{X}(s)$ in Eq. (3) is independent of the variable ϑ and is thus taken out of the integration. In addition, we assume zero initial conditions, i.e., $\mathbf{x}(0) = \mathbf{0}$, which leads to the characteristic equation of the system Eq. (1) as

$$\mathcal{F}(s, \tau_1, \tau_2) = \det\left(s\mathbf{I} - \mathbf{A} + \frac{\mathbf{B}}{s}\left(e^{-\tau_2 s} - e^{-\tau_1 s}\right)\right) = 0. \tag{4}$$

The characteristic Eq. (4) is not well-posed at $s = 0$ since s appears in the denominator. Consequently, one should carefully examine the spectrum of Eq. (4) near $s = 0$, namely, $s \to 0$.

Observation 1. Since both the numerator and denominator of $\frac{e^{-\tau_2 s} - e^{-\tau_1 s}}{s}$ move towards zero as $s \to 0$, the second-order Taylor series approximation is applied for the replacement of the exponential term in Eq. (4),

$$e^{-\tau_k s} \cong 1 - \tau_k s + \frac{(\tau_k s)^2}{2!}, |\tau_k s| \ll 1, k = 1, 2, \tag{5}$$

resulting in

$$\mathcal{F}_T(s \to 0, \tau_1, \tau_2) = \det\left(s\mathbf{I} - \mathbf{A} - \mathbf{B}(\tau_2 - \tau_1) + s\mathbf{B}\left(\frac{\tau_2^2 - \tau_1^2}{2}\right)\right) = 0. \tag{6}$$

Then, we have

$$\mathcal{F}_T^{s\to 0}(\Delta\tau) = \det(-\mathbf{A} - \mathbf{B}\Delta\tau) = 0 \tag{7}$$

where $\Delta\tau = \tau_2 - \tau_1$. Evidently, an extra stability boundary in the delay domain emerges, which is associated with the root crossings when $s = \omega i \to 0$, $i = \sqrt{-1}$. Such a singularity should be particularly discussed in the analysis considering that the stability reversal may take place when the delay pair (τ_1, τ_2) crosses the solutions of Eq. (7), which is the first technical issue of this study.

To proceed, let us focus on $\omega > 0$ and define the complete set of the imaginary eigenvalues of Eq. (4) for all the possible variations of the delay vector $\boldsymbol{\tau} = (\tau_1, \tau_2) \in \mathbb{R}^{2+}$ as

$$\boldsymbol{\Omega}_{\mathcal{F}} = \left\{\omega \mid \mathcal{F}(s = \omega i, \boldsymbol{\tau}) = 0, \omega > 0, \boldsymbol{\tau} \in \mathbb{R}^{2+}\right\}. \tag{8}$$

Then, tracking all the feasible triplets (ω, τ_1, τ_2) in (8) is the second technical issue for a complete stability analysis. In fact, the KOH are generated by all these triplets as per Definition 3 and Definition 4 given in Appendix. In the sequel, both of these two technical issues are addressed.

3. Main results

3.1. Equivalent system and standing root analysis

The existence of the variable s in the denominator of Eq. (4) brings inconvenience to the analysis, hence we present the following lemma.

Lemma 1. *The stability feature of the system Eq. (1) is equivalent to that of the following system with two lumped delays*

$$\ddot{\mathbf{x}}(t) - \mathbf{A}\dot{\mathbf{x}}(t) + \mathbf{B}[\mathbf{x}(t - \tau_2) - \mathbf{x}(t - \tau_1)] = 0. \tag{9}$$

Proof. Notice that the characteristic equation of the system Eq. (9) is

$$\mathcal{H}(s, \tau_1, \tau_2) = \det\left(s^2\mathbf{I} - s\mathbf{A} + \mathbf{B}\left(e^{-\tau_2 s} - e^{-\tau_1 s}\right)\right) = 0. \tag{10}$$

We have the following equation due to the determinant properties

$$\mathcal{H}(s, \tau_1, \tau_2) = s^n \mathcal{F}(s, \tau_1, \tau_2), \tag{11}$$

which means that Eq. (10) possesses all the eigenvalues of Eq. (4) plus n additional roots at $s = 0$. In fact, $\mathcal{H}(s, \tau_1, \tau_2) = 0$ holds for any delay compositions when $s = 0$, implying that these additional roots are invariant for $\boldsymbol{\tau} \in \mathbb{R}^{2+}$ and thus denoted as *stationary roots*. It follows that

$$\boldsymbol{\Omega}_{\mathcal{F}} = \boldsymbol{\Omega}_{\mathcal{H}} - \{\omega \mid \mathcal{H}(s = \omega i = 0, \boldsymbol{\tau}) = 0\} \tag{12}$$

where

$$\boldsymbol{\Omega}_{\mathcal{H}} \triangleq \left\{\omega \mid \mathcal{H}(s = \omega i, \boldsymbol{\tau}) = 0, \omega \geqslant 0, \boldsymbol{\tau} \in \mathbb{R}^{2+}\right\}. \tag{13}$$

Therefore, the stability outlook of Eq. (1) is equivalent to that of Eq. (9) by excluding these stationary roots. The proof is finished. □ □

Remark 2. We refer to Eqs. (9) and (10) as the equivalent system and equivalent characteristic equation, respectively. Then, the availability of the second derivative of the state, $\ddot{\mathbf{x}}(t)$ in Eq. (9), is unneeded since the equivalent system Eq. (9) is proposed for the ease of the stability assessment in the frequency domain. Indeed, the time-domain simulations in Section 4 are developed using the original system Eq. (1), c.f. [5].

Remark 3. It is sufficient to employ the non-negative frequencies in the frequency sweeping framework thanks to the conjugate symmetry of the complex variable s, leading to $\omega \geq 0$ in Eq. (13). However, the singularity enforces $s \neq 0$ in Eq. (4) and thus ω is strictly positive in Eq. (8).

Now, readers may wonder how to detect the singular stability crossings using the equivalent characteristic Eq. (10), i.e., the above-mentioned first technique issue. The associated realization leads to the following standing root analysis procedure. Although we discard these stationary roots as per Lemma 1, it is possible for some other eigenvalues to cross the origin to the right (or left) half-plane, which is regarded as a standing root case [5,24]. When such crossings occur, $s = 0$ becomes a multiple root with multiplicity more than n. In other words, only one characteristic root at $s = 0$ would move as the delay varies while the other n stationary roots remain identical. Hence, we have to check the higher-order derivatives of the equivalent characteristic Eq. (10) with respect to s to detect such zero-root crossings.

Definition 1 (. *Potential Stability Changing Curves (PSCC)*) The PSCC of the considered system are defined as the union of the KOH and standing root boundary (SRB), which is determined by

$$\left.\frac{\partial^n \mathcal{H}(s, \tau_1, \tau_2)}{\partial s^n}\right|_{s=0} = 0. \tag{14}$$

The SRB can be alternatively obtained by Eq. (7) since the solutions of Eq. (14) are identical to those of Eq. (7). In other words, the crossing behavior at $s = 0$ in Eq. (10) correlates with the extreme situation where $s \to 0$ in Eq. (4). Next, the crossings are judged as stabilizing or destabilizing by the root tendency (RT) concept. For an ordinary imaginary root, we have

$$\mathrm{RT} = \mathrm{sgn}\left[\Re\mathfrak{e}\left(\left.\frac{\partial s}{\partial \tau_k}\right|_{s=\omega i}\right)\right] = \mathrm{sgn}\left[\Re\mathfrak{e}\left(\left.\frac{-\partial \mathcal{H}(s, \tau_1, \tau_2)/\partial \tau_k}{\partial \mathcal{H}(s, \tau_1, \tau_2)/\partial s}\right|_{s=\omega i}\right)\right]. \tag{15}$$

However, for the SRB, $s = 0$ is a multiple root so that both $\partial \mathcal{H}(s, \tau_1, \tau_2)/\partial \tau_k$ and $\partial \mathcal{H}(s, \tau_1, \tau_2)/\partial s$ vanish, namely, the implicit function theorem [25] is no longer valid. Therefore, we resort to the characteristic equation derived from the Taylor expansion in Eq. (6),

leading to

$$\mathrm{RT}_{SRB} = \mathrm{sgn}\left[\Re\mathfrak{e}\left(\frac{-\partial \mathcal{F}_T(s\to 0,\tau_1,\tau_2)/\partial \tau_k}{\partial \mathcal{F}_T(s\to 0,\tau_1,\tau_2)/\partial s}\bigg|_{s=\omega i\to 0}\right)\right]. \tag{16}$$

That completes the standing root analysis.

Remark 4. The RT concept given in Definition 5 and Proposition 2 in Appendix is invalid when the first derivative in Eq. (44) vanishes or the imaginary eigenvalue is multiple. Actually, the crossing behavior of the SRB can be analyzed directly with the equivalent characteristic Eq. (10). Besides, multiple characteristic roots may cross the origin to the right (or left) half-plane for certain cases, which is kept outside the scope of the text. Interested readers are referred to [6,14,26] for a more meticulous treatment of such multiple identical imaginary roots.

3.2. Dixon resultant-based frequency sweeping procedure

The frequency sweeping technique is deployed to calculate the KOH, i.e., the second technique issue, since the complete stability map necessitates both the SRB and KOH as per Definition 1. Nevertheless, we wish to avoid sweeping ω from 0^+ to $+\infty$ to boost computational efficiency, which in turn entails the exact feasible range of $\mathbf{\Omega}_{\mathcal{H}}$. Hence, we present some preparatory steps as follows before revealing the main results.

3.2.1. Transformation of the characteristic equation

We substitute $s=\omega i$ to Eq. (10) since the KOH correspond to the delay compositions that exhibit purely imaginary roots. Besides, the Rekasius substitution is utilized to replace the transcendental terms in Eq. (10):

$$e^{-\tau_k s} = \frac{1-T_k s}{1+T_k s},\quad T_k\in\mathbb{R},\quad k=1,2, \tag{17}$$

which is exact when $s=\omega i$. Accordingly, the multivalued inverse mapping from T_k to τ_k is

$$\tau_k = \frac{2}{\omega}\left[\tan^{-1}(T_k\omega)+l\pi\right],\quad k=1,2,\quad l=0,1,2,\cdots. \tag{18}$$

The following modified quasi-polynomial function is obtained by substituting Eq. (17) into Eq. (10) and eliminating $1+T_k\omega i$ terms in the denominators:

$$\hat{\mathcal{H}}(\omega i,T_1,T_2) = \mathcal{H}(\omega i,T_1,T_2)\times\prod_{k=1}^{2}(1+T_k\omega i)^c = 0 \tag{19}$$

where $c=\mathrm{rank}(\mathbf{B})$ is the commensurate degree of τ_k, $k=1,2$. For the complex Eq. (19) to hold, its real and imaginary parts should vanish, i.e., $p_{\mathcal{R}}(\omega,T_1,T_2)\triangleq\Re\mathfrak{e}\left(\hat{\mathcal{H}}\right)=0$, $p_{\mathcal{I}}(\omega,T_1,T_2)\triangleq\Im\mathfrak{m}\left(\hat{\mathcal{H}}\right)=0$. Then, $p_{\mathcal{R}}$ and $p_{\mathcal{I}}$ are rewritten as the polynomials with respect to T_2:

$$p_{\mathcal{R}}(\omega,T_1,T_2) = \sum_{j=0}^{c} a_j(\omega,T_1)T_2^j = 0, \tag{20}$$

$$p_{\mathcal{I}}(\omega, T_1, T_2) = \sum_{j=0}^{c} b_j(\omega, T_1) T_2^j = 0 \tag{21}$$

where $a_j(\omega, T_1)$ and $b_j(\omega, T_1)$ are the corresponding real coefficients parameterized in T_1 and ω. It should be noted that the common $(\omega, T_1, T_2) \in \mathbb{R}^3$ solutions of Eqs. (20) and (21) lead to $(\omega, \tau_1, \tau_2) \in \mathbb{R}^3$ by Eq. (18), which carry the complete information of the KOH. Hence, the problem is transformed into acquiring all the common nontrivial solutions of Eqs. (20) and (21) in the entire (T_1, T_2) plane.

3.2.2. Dixon resultant theory

A powerful, efficient mathematical tool called Dixon resultant theory [27] is developed to disclose the necessary condition for the existence of a common zero of a set of polynomials. We prefer this tool because of its higher computational efficiency over peer methodologies [28]. In the sequel, let us introduce the Dixon resultant-based frequency sweeping routine.

To start with, the common $T_2 \in \mathbb{R}$ root of Eqs. (20) and (21) is checked. We present the following **Dixon polynomial**, bearing in mind that Eqs. (20) and (21) are polynomials in T_2 with coefficients parametrized in ω and T_1:

$$\delta(T_2, \alpha) = \frac{1}{(T_2 - \alpha)} \begin{vmatrix} p_{\mathcal{R}}(\omega, T_1, T_2) & p_{\mathcal{I}}(\omega, T_1, T_2) \\ p_{\mathcal{R}}(\omega, T_1, \alpha) & p_{\mathcal{I}}(\omega, T_1, \alpha) \end{vmatrix}, \tag{22}$$

where $p_{\mathcal{R}}(\omega, T_1, \alpha)$ and $p_{\mathcal{I}}(\omega, T_1, \alpha)$ stand for replacing T_2 with a dummy variable α. Notice that Eq. (22) is symmetric with respect to T_2 and α, i.e., $\delta(\alpha, T_2) = \delta(T_2, \alpha)$. By defining

$$d_{\max} = \max[\deg(p_{\mathcal{R}}), \deg(p_{\mathcal{I}})] \tag{23}$$

as the maximum degree of T_2 in these two polynomials, we obtain that δ is of degree $d_{\max} - 1$ in α. Since each common T_2 root of Eqs. (20) and (21) makes $\delta(T_2, \alpha)$ equal to zero, the coefficients of all the powers of α in $\delta(T_2, \alpha)$ should be zero at this common root. We then have $d_{\max}$ equations associated with the coefficients of $\alpha^i (i = 0, 1, \cdots, d_{\max} - 1)$, all of which are polynomials in T_2. Formatting these equations in the matrix form yields

$$\mathbf{F}_1(\omega, T_1) \begin{pmatrix} 1 \\ T_2 \\ \vdots \\ T_2^{d_{\max}-1} \end{pmatrix} = \begin{pmatrix} 0 \\ 0 \\ \vdots \\ 0 \end{pmatrix} \tag{24}$$

where $\mathbf{F}_1(\omega, T_1) \in \mathbb{R}^{d_{\max} \times d_{\max}}$ is the coefficient matrix of these $d_{\max}$ equations, known as the **Dixon matrix**. For Eq. (24) to hold, $\mathbf{F}_1(\omega, T_1)$ has to be singular, i.e.,

$$R_{T_2}(\omega, T_1) \triangleq \det[\mathbf{F}_1(\omega, T_1)] = 0. \tag{25}$$

We end up having an equation in terms of only two variables, i.e., ω and T_1, implying that T_2 is eliminated using Eqs. (20) and (21).

Remark 5. It is obvious from Eq. (25) that if the lower and upper frequency bounds are known, one can sweep $\omega > 0$ in this interval and calculate the corresponding $T_1 \in \mathbb{R}$ values. Next, the solutions of $T_2 \in \mathbb{R}$ can be obtained using Eqs. (20) and (21) with the knowledge of $(\omega, T_1) \in \mathbb{R}^2$. Then, all the delay components of the KOH are determined by the mapping Eq. (18) with the corresponding ω.

Remark 6. In fact, one may routinely adopt the famous Sylvester resultant method as per [12] for the complete stability analysis of the LTI time-delay dynamics, even for the very recent results such as [22,29,30]. In this manner, the equivalent solutions of Eq. (25) are generated by calculating the determinant of the Sylvester matrix of Eqs. (20) and (21) with respect to T_2, denoted as $\mathbf{S}_1(\omega, T_1)$. However, the authors strongly recommend the Dixon resultant method due to its higher efficiency to handle increasingly complicated cases. To this end, comparisons between these two methods are provided in Section 4 to show the computational edge of our theory.

We next explore how to pinpoint the exact bounds of ω that carries the crucial information of the KOH. For this, we check the extremum of ω, which entails the following condition

$$\frac{d\omega}{dT_1} = 0. \tag{26}$$

We then take the total derivative of the left-hand side of Eq. (25):

$$dR_{T_2} = \frac{\partial R_{T_2}}{\partial \omega} d\omega + \frac{\partial R_{T_2}}{\partial T_1} dT_1 = 0, \tag{27}$$

to find the condition that satisfies both Eqs. (25) and (26) simultaneously, which results in

$$\frac{d\omega}{dT_1} = -\frac{\frac{\partial R_{T_2}}{\partial T_1}}{\frac{\partial R_{T_2}}{\partial \omega}}. \tag{28}$$

We obtain

$$\mathscr{D} R_{T_2}(\omega, T_1) \triangleq \frac{\partial R_{T_2}}{\partial T_1} = 0 \tag{29}$$

by excluding the extremely rare cases that $\frac{\partial R_{T_2}}{\partial \omega} = 0$. We now end up having Eqs. (25) and (29) at our disposal, both of which are in terms of ω and T_1. In order to find their common $T_1 \in \mathbb{R}$ solutions, we rewrite these two equations as polynomials in T_1 with parameters in ω and apply the above-mentioned Dixon resultant procedure one more time.

Definition 2 (. *Discriminant of* $R_{T_2}(\omega, T_1)$) The discriminant of $R_{T_2}(\omega, T_1)$ with respect to T_1, denoted as $D_{T_1}(\omega)$, is the resultant of the two polynomials in Eqs. (25) and (29) by eliminating T_1.

Note that $D_{T_1}(\omega)$ is a function of only one variable ω. Then, the following theorems are formulated to reveal the exact frequency range.

Theorem 1. *The exact lower bound of* $\mathbf{\Omega}_{\mathcal{H}}$ *for the equivalent system Eq. (9) is always zero.*

Proof. It is observed that $s = 0$ holds for the equivalent characteristic Eq. (10) under any circumstances, leading to the vanishment of both Eqs. (20) and (21) for $s = 0$. □ □

Theorem 2. *The exact upper bound of* $\mathbf{\Omega}_{\mathcal{H}}$ *for the equivalent system Eq. (9) is the maximum positive real root* $\omega \in \mathbb{R}^+$ *with the corresponding* $(T_1, T_2) \in \mathbb{R}^2$ *for* $D_{T_1}(\omega)$.

Proof. The imaginary spectra for Eq. (10) are equivalent to those for (19) due to the exact Rekasius substitution. First, the common solutions for $T_2 \in \mathbb{R}$ of Eqs. (20) and (21) entail Eq. (25). Second, the extremum condition dictates the condition Eq. (26) which leads to Eq. (29). Then, the discriminant of the resultant $R_{T_2}(\omega, T_1)$, i.e., $D_{T_1}(\omega)$ should vanish to

simultaneously meet the conditions in Eqs. (25) and (29) concurrently. Besides, both T_1 and T_2 should be real and correspond to $\omega \in \mathbb{R}^+$during all the above operations according to Eq. (17) and (18). We declare that the positive real solutions of $D_{T_1}(\omega)$ corresponding to $(T_1, T_2) \in \mathbb{R}^2$ dictate the extrema candidates. Therefore, the maximum solution $\omega \in \mathbb{R}^+$ of $D_{T_1}(\omega)$ with the corresponding $(T_1, T_2) \in \mathbb{R}^2$ determines the upper bounds of $\mathbf{\Omega}_{\mathcal{H}}$. □ □

We are able to find the exact frequency range of $\mathbf{\Omega}_{\mathcal{H}}$ as per Theorems 1 and 2. Then, we deploy the frequency sweeping technique over this admissible range to generate the KOH. Last, the CTCR paradigm is employed for the stability evaluation of the PSCC, i.e., the union of the KOH and SRB, leading to the complete stability map in the delay domain.

Remark 7. For the extension of the lumped control law Eq. (2) to the one with multiple delays, the number of the delays in the equivalent system becomes no less than four, then the analysis in the entire delay domain is almost computationally infeasible. Therefore, fixing all but two of the delays would be more efficient and could facilitate visualization by creating a 2-D cross section of the stability map. Please refer to our most recent work [31] for this extension following the ideas in [12] and [20].

Remark 8. Our work can be extended by considering the time-varying delays instead of the constant delays, which is more realistic [10]. However, omitting the time-varying effect is a common practice for the frequency-domain approaches. Remarkably, it is possible to further scrutinize the *slowly* time-varying delays following the work [32], which establishes the connections between the time domain and the frequency domain. Then, only the *sufficient* condition for the asymptotic stability is given by the equivalent analysis while our treatment for the system of interest with constant delays guarantees the *necessary and sufficient* condition.

4. Case study

In this section, two example cases are provided. In the first one, more intermediate steps of the Dixon resultant are given for the illustrative purpose. The second one shows that our proposed procedure is still applicable for the higher dimensional system. Especially, two points are noteworthy. First, it is feasible for the distributed control strategy in Eq. (1) to enhance the delay robustness of the system. Second, the superiority of the Dixon resultant-based procedure over the Sylvester resultant-based one in computational efficiency is specifically emphasized.

4.1. Case 1

The first example case is presented in the form of Eq. (1) with the following matrices

$$\mathbf{A} = \begin{pmatrix} -10 & 0 & 0 \\ -3.2 & -23.2 & -3.2 \\ 0 & 0 & -20 \end{pmatrix}, \mathbf{B} = \begin{pmatrix} 0 & 20 & 0 \\ 10 & 0 & 10 \\ 0 & 20 & 0 \end{pmatrix}. \tag{30}$$

The equivalent characteristic equation in Eq. (10) is written as

$$\begin{aligned} \mathcal{H}(s, \tau_1, \tau_2) = {} & s^6 + 53.2\,s^5 + 896\,s^4 + \left(4640e^{2(\tau_1+\tau_2)s} - 128e^{(2\tau_1+\tau_2)s} + 128e^{(\tau_1+2\tau_2)s}\right)e^{-2(\tau_1+\tau_2)s}s^3 \\ & + \left(-400e^{2\tau_1 s} - 400e^{2\tau_2 s} + 800e^{(\tau_1+\tau_2)s} - 1920e^{(2\tau_1+\tau_2)s} + 1920e^{(\tau_1+2\tau_2)s}\right)e^{-2(\tau_1+\tau_2)s}s^2 \\ & + \left(-6000e^{2\tau_1 s} - 6000e^{2\tau_2 s} + 12000e^{(\tau_1+\tau_2)s}\right)e^{-2(\tau_1+\tau_2)s}s. \end{aligned} \tag{31}$$

We observe that Eq. (31) contains commensurate delay terms, e.g., $e^{2\tau_1 s}$, cross-talk terms, e.g., $e^{(\tau_1+\tau_2)s}$, and cross-talk with commensuracy terms, e.g., $e^{(2\tau_1+\tau_2)s}$. The non-delayed system in

Eq. (31) corresponding to $\tau_1 = \tau_2 = 0$ has six characteristic roots at -10, -20, -23.2, and 0 with multiplicity 3. Thus, $\mathbf{A}$ is Hurwitz by discarding these stationary roots. We next write Eqs. (20) and (21) as the following noticing that $c = \text{rank}(\mathbf{B}) = 2$:

$$p_{\mathcal{R}}(\omega, T_1, T_2) = a_0 + a_1 T_2 + a_2 T_2^2, \tag{32}$$

$$p_{\mathcal{I}}(\omega, T_1, T_2) = b_0 + b_1 T_2 + b_2 T_2^2 \tag{33}$$

where a_j and b_j, $j = 0, 1, 2$, are the corresponding real coefficients parameterized in T_1 and ω, leading to the Dixon polynomial in Eq. (22) as

$$\begin{aligned}\delta(T_2, \alpha) = &((a_1 b_0 - a_0 b_1) + (a_2 b_0 - a_0 b_2) T_2) \\ &+((a_2 b_0 - a_0 b_2) + (a_2 b_1 - a_1 b_2) T_2)\alpha = 0\end{aligned} \tag{34}$$

with $d_{\max} = 2$ in Eq. (23). The associated Dixon matrix is given by

$$\mathbf{F}_1 = \begin{pmatrix} a_1 b_0 - a_0 b_1 & a_2 b_0 - a_0 b_2 \\ a_2 b_0 - a_0 b_2 & a_2 b_1 - a_1 b_2 \end{pmatrix} \in \mathbb{R}^{2\times 2} \tag{35}$$

since each common T_2 root of Eqs. (32) and (33) is a solution of Eq. (34) independently from α, leading to

$$R_{T_2}(\omega, T_1) = \det(\mathbf{F}_1) = -a_0^2 b_2^2 - a_2^2 b_0^2 - a_0 a_2 b_1^2 - b_0 b_2 a_1^2 + a_0 a_1 b_1 b_2 + a_1 a_2 b_0 b_1 + 2 a_0 a_2 b_0 b_2. \tag{36}$$

Let us remark that T_2 is eliminated from the aforementioned steps. We then calculate $\mathscr{D} R_{T_2}(\omega, T_1)$ in Eq. (29). We focus on T_1 and form the Dixon matrix again using $R_{T_2}(\omega, T_1)$ and $\mathscr{D} R_{T_2}(\omega, T_1)$, denoted as $\mathbf{F}_2 \in \mathbb{R}^{8\times 8}$. Then,

$$D_{T_1}(\omega) = \det(\mathbf{F}_2) = 0. \tag{37}$$

It is found that $\omega = 2.6650$ is the maximum positive real root of Eq. (37) that corresponds to $(T_1, T_2) \in \mathbb{R}^2$. Hence, the exact range of $\mathbf{\Omega}_{\mathcal{H}}$ is determined as $[0, 2.6650]$ as per Theorems 1 and 2. We can obtain the KOH in the delay domain by deploying the frequency sweeping procedure presented in Remark 5. Furthermore, the SRB is generated by Eq. (14) as

$$\frac{25}{8}\tau_1^2 + \frac{25}{8}\tau_2^2 - \frac{25}{4}\tau_1\tau_2 + \tau_1 - \tau_2 - \frac{29}{12} = 0, \tag{38}$$

which is a quadratic equation with respect to τ_1 and τ_2. The complete stability map is shown in Fig. 1 with the employment of the CTCR paradigm using these PSCC, i.e., the union of the KOH and SRB.

As depicted, the SRB in (38) is divided into two segments with opposite RT values. However, only the upper left half of the stability map is significant due to the ordering relation between the distributed delay bounds, i.e., $\tau_2 > \tau_1$. A small stable strip exists just over the $\tau_1 = \tau_2$ line as observed from Fig. 1. This observation points to the fact that the delayed feedback control fails to provide enough strength to destabilize the system against the Hurwitz system matrix $\mathbf{A}$ if $\Delta\tau = \tau_2 - \tau_1$ is sufficiently small. In light of this, we next present how to stabilize the system of interest even if the inherent delay τ_1 is large, i.e., in the order of 1s. Once τ_1 is detected, the compensatory delay τ_2 should be slightly larger than τ_1 so that the delay composition (τ_1, τ_2) falls into the valid stable regions of the stability

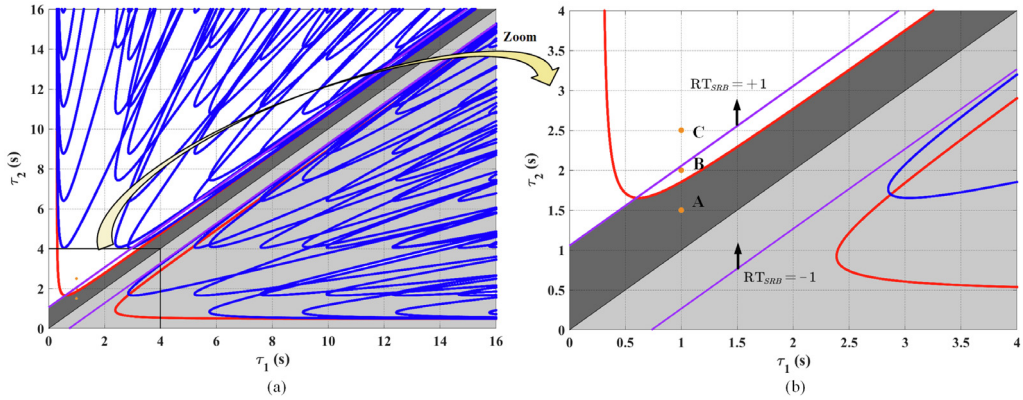

Fig. 1. (a) Complete stability map for Case 1; (b) Zoomed-in view of the stability map; Red, blue, and purple curves are the KH, OH, and SRB, respectively; Dark shaded regions are stable; Light shaded regions are insignificant. (For interpretation of the references to colour in this figure legend, the reader is referred to the web version of this article.)

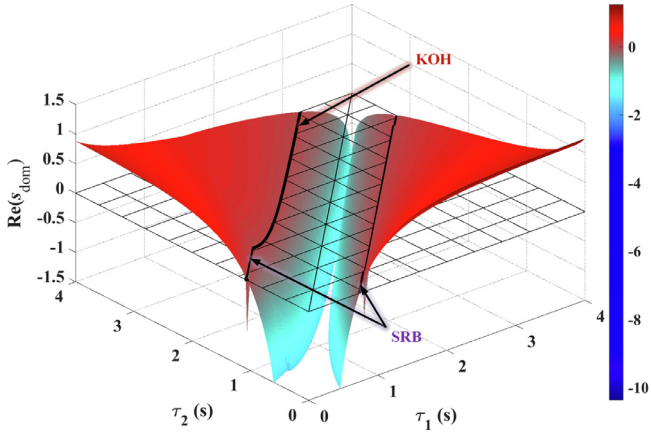

Fig. 2. Real parts of the rightmost characteristic roots of Eq. (4) for Case 1 with respect to τ_1 and τ_2.

map. Considering that the system could be stabilized without tuning the gains, the distributed control strategy in Eq. (1) offers us an alternative way for enhancing the delay robustness.

A numerical routine called Quasi-Polynomial mapping-based Root-finder (QPmR) [33] is used over the original characteristic equation in Eq. (4) to verify the effectiveness of the obtained stability map in Fig. 1. Essentially, this routine computes all the zeros of a quasi-polynomial function within a given region in the complex plane. Consequently, we declare the test point to be stable if the rightmost characteristic root, denoted as s_{dom}, for a certain delay composition has a negative real part. Otherwise, the point is unstable. Fig. 2 shows the variation of the real parts of the rightmost characteristic roots, say, $\mathrm{Re}(s_{dom})$, with respect to various delay compositions within the zone of interest. It is obvious that the stable region in Fig. 1 coincides completely with the zone where $\mathrm{Re}(s_{dom}) < 0$ and thus the stability map is validated. In particular, both the segments of the KOH and SRB are identified in Fig. 2.

Three representative points marked as A, B, and C in Fig. 1 are examined to further study the root-crossing behavior associated with the PSCC. The results of the Simulink-based

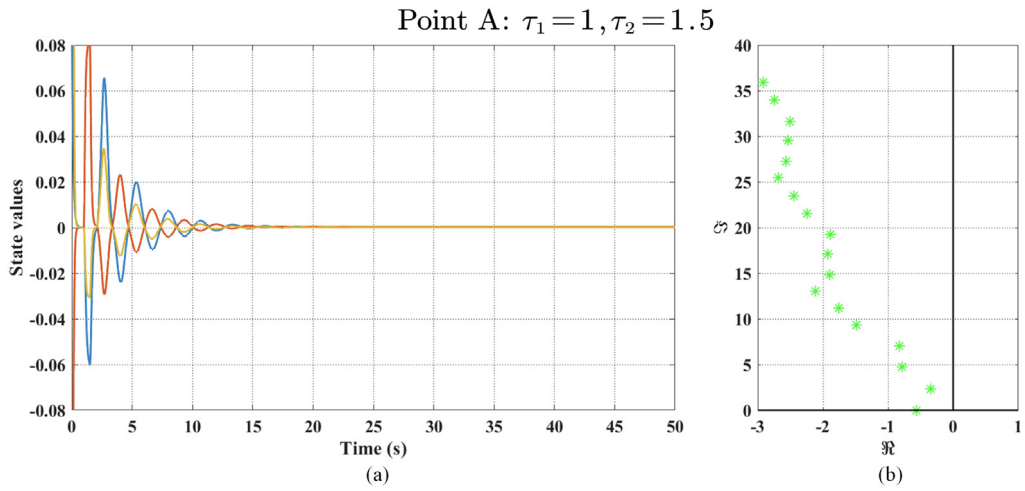

Fig. 3. Dynamic analysis for Case 1 with $\tau_1 = 1$ and $\tau_2 = 1.5$; (a) System response of Eq. (1) to nonzero initial conditions obtained through numerical simulations; (b) Spectrum of the original characteristic Eq. (4) using the QPmR routine ($*$ - stable characteristic roots).

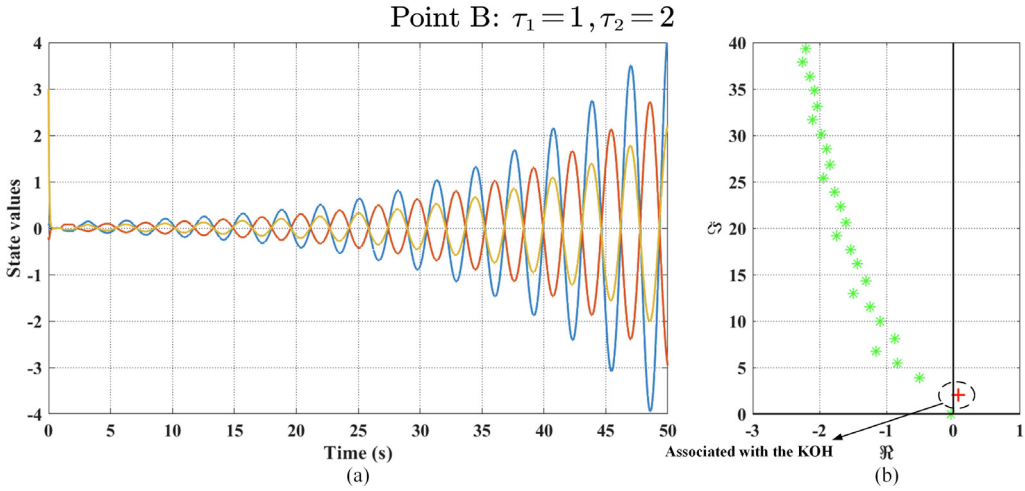

Fig. 4. Dynamic analysis for Case 1 with $\tau_1 = 1$ and $\tau_2 = 2$; (a) System response of Eq. (1) to nonzero initial conditions obtained through numerical simulations; (b) Spectrum of the original characteristic Eq. (4) using the QPmR routine ($*$ - stable characteristic roots; $+$ - unstable characteristic roots).

simulations for Case 1 as well as the spectrum distribution using the QPmR routine for points A, B, and C are shown in Figs. 3–5, respectively. As observed, for $\tau_1 = 1$, the destabilizing crossings related to the KOH and SRB occur in succession if τ_2 is chosen as 1.5 and gradually increases to 2.5. Notice that the destabilizing crossing associated with the KOH leads to a pair of conjugate unstable roots, while the an associated with the SRB results in an unstable root on the real axis. Accordingly, the dynamic response of the system in Eq. (1) is stable for point A, whereas it is unstable for points B and C. These results reconfirm the stability map shown in Fig. 1.

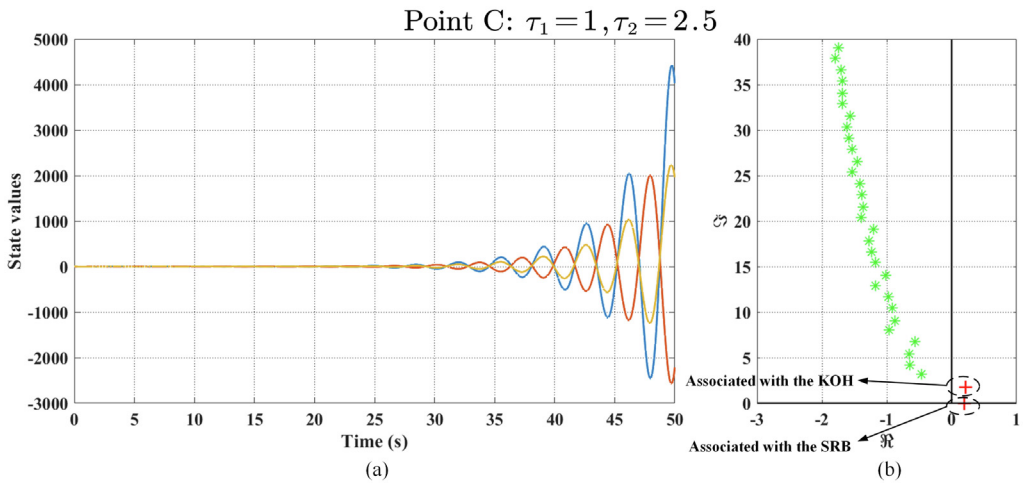

Fig. 5. Dynamic analysis for Case 1 with $\tau_1 = 1$ and $\tau_2 = 2.5$; (a) System response of Eq. (1) to nonzero initial conditions obtained through numerical simulations; (b) Spectrum of the original characteristic Eq. (4) using the QPmR routine ($*$ - stable characteristic roots; $+$ - unstable characteristic roots).

Table 1
Stability chart of the lumped control strategy in Eq. (2) for Case 1.

τ_1 range (s)	Stable / Unstable	Number of unstable roots
[0, 0.1979]	S	0
[0.1979, 0.7078]	U	2
[0.7078, 1.2177]	U	4
[1.2177, 1.7276]	U	6
[1.7276, 2.2375]	U	8
⋮	⋮	⋮

We next match this distributed control strategy against the lumped one concerning the delay robustness. The complete stability problem of the lumped control strategy is extensively studied. Then, the exact stability pockets of Eq. (2) with the system matrices (30) are examined by the method in [16], leaving the details to the reference. The corresponding stability chart is shown below. Clearly, the stability of the lumped control law could not be recovered for $\tau_1 > 0.1979$. The difference in the delay robustness between these two control strategies is self-evident by revisiting the stability map shown in Fig. 1.

Finally, we evaluate the efficiency for computing the resultants of these polynomial equations. As mentioned in Remark 6, both $R_{T_2}(\omega, T_1)$ and $D_{T_1}(\omega)$ can be formulated using the Sylvester-type resultant method. For this, let us write the Sylvester matrix of Eqs. (32) and (33) with respect to T_2 as

$$\mathbf{S}_1 = \begin{pmatrix} a_2 & a_1 & a_0 & 0 \\ 0 & a_2 & a_1 & a_0 \\ b_2 & b_1 & b_0 & 0 \\ 0 & b_2 & b_1 & b_0 \end{pmatrix} \in \mathbb{R}^{4\times 4}, \tag{39}$$

Table 2
Comparisons of the time and memory usage between the Dixon-type resultant method and the Sylvester-type one for Case 1.

	Dixon-type resultant method	Sylvester-type resultant method
The first resultant step to obtain $R_{T_2}(\omega, T_1)$		
Dimensions of the matrix	$\mathbf{F}_1 : 2 \times 2$	$\mathbf{S}_1 : 4 \times 4$
Memory used	172.27 KiB	341.87 KiB
CPU time	0 ns	0 ns
The second resultant step to obtain $D_{T_1}(\omega)$		
Dimensions of the matrix	$\mathbf{F}_2 : 8 \times 8$	$\mathbf{S}_2 : 15 \times 15$
Memory used	145.69 MiB	1863.68 MiB
CPU time	0.765 s	13.34 s

and then calculate its determinant. In this manner, we have $\det(\mathbf{S}_1) = -\det(\mathbf{F}_1)$ (Table 1). Similarly, the Sylvester matrix of $R_{T_2}(\omega, T_1)$ and $\mathscr{D}R_{T_2}(\omega, T_1)$ concerning T_1 is obtained as $\mathbf{S}_2 \in \mathbb{R}^{15\times 15}$, the determinant of which gives an equivalent equation to Eq. (37). The time and memory usage for calculating the determinant is measured by executing the "Usage" routine of Maple 2020, then the outcomes are shown in Table 2.

Note that 1GiB = 1024MiB, 1MiB = 1024KiB. Besides, we run the computations on a standard PC with a 3.6 GHz processor (8 cores), utilizing 31.4 GiB of RAM. The superiority of the Dixon resultant in computational efficiency vis–vis the Sylvester resultant is easy to check from Table 2. Surprisingly, the proposed Dixon resultant shortens the computation time by 16.44 times when computing $D_{T_1}(\omega)$.

4.2. Case 2

The ensuing example is provided to demonstrate that the proposed procedure is capable of handling higher dimensional systems:

$$\mathbf{A} = \begin{pmatrix} -0.1 & 0.1 & 0 & 0 & 0 & 0.1 & 0.1 \\ 0 & -3 & 3 & 0 & 0 & 0 & 0 \\ -12 & 0 & -0.1 & -0.75 & 0.1 & 0 & 0 \\ -72 & 0 & 0 & -5 & -0.8 & 0 & 0 \\ -1 & 0 & 0 & 0 & 0 & 0 & 0 \\ 0 & 0 & 0 & 0 & 0 & -20 & 0 \\ 0 & 0 & 0 & 0 & 0 & 0 & -20 \end{pmatrix},$$

$$\mathbf{B} = \begin{pmatrix} 0 & -0.1 & 0 & 0 & 0 & 0 & 0 \\ 0 & 0.05 & 0 & 0 & 0 & 0 & 0 \\ 0 & 0 & 0 & 0 & 0.01 & 0 & 0 \\ 0 & 0 & 0 & 0 & 0.01 & 0 & 0 \\ 0 & 0 & 0 & 0 & 0.05 & 0 & 0 \\ -20 & 0 & 0 & 0 & 0.2 & 0 & 0 \\ 0 & 0 & 0 & 0 & -0.05 & 0 & 0 \end{pmatrix}. \tag{40}$$

Notice that $\operatorname{rank}(\mathbf{A}) = 7$, $\operatorname{rank}(\mathbf{B}) = 3$. For $\tau_1 = \tau_2 = 0$, the equivalent characteristic equation in (40) has fourteen characteristic roots at -0.2682, -2.4931, -5.2815,

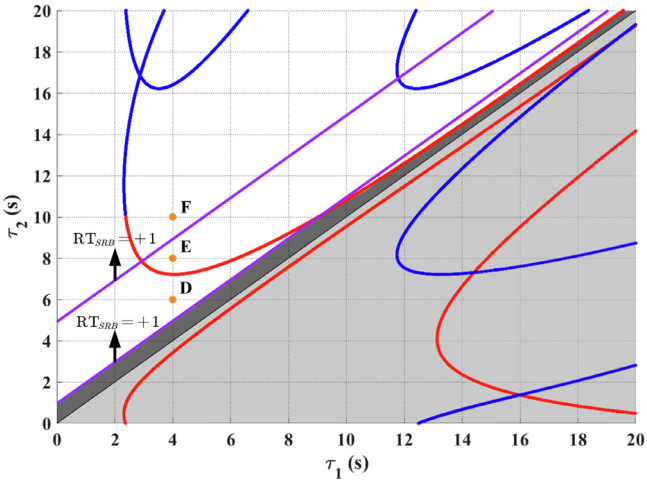

Fig. 6. Complete stability map for Case 2; Red, blue, and purple curves are the KH, OH, and SRB, respectively; The dark shaded region is stable; The light shaded region is insignificant. (For interpretation of the references to colour in this figure legend, the reader is referred to the web version of this article.)

$-0.0785\pm0.2953i$, -20 with multiplicity 2, and 0 with multiplicity 7. The bounds of $\mathbf{\Omega}_{\mathcal{H}}$ is then determined as $[0, 0.7128]$, which yields the KOH. Besides, the SRB is given as

$$\tau_1^3 - \tau_2^3 - 3\,\tau_1^2\,\tau_2 + 3\,\tau_1\,\tau_2^2 - 558.85\tau_1^2 - 558.85\tau_2^2 + 1117.7\tau_1\,\tau_2 \\ -3309\,\tau_1 + 3309\,\tau_2 - 2640 = 0, \tag{41}$$

which is a cubic equation with respect to τ_1 and τ_2. Actually, the degree of the SRB equation is determined by the rank of the delayed feedback gain matrix, i.e., rank$(\mathbf{B})$, which can be inferred from Eq. (7) directly. However, not all the solutions of the SRB equation are valid. For instance, we obtain τ_2 as 4.9507, 8.9171, and -560.7178 (invalid) by fixing $\tau_1 = 4$ in Eq. (41). Next, the corresponding stability map is shown in Fig. 6. It is remarkable that only two segments of the SRB are found in Fig. 6, both of which correspond to destabilizing crossings. We underline that the RTs of the PSCC should be evaluated correctly. For example, one may declare an incorrect stability map with an extra, mistakenly judged stable region if the upper segment of the SRB in Fig. 6 is determined to be stabilizing.

Next, the spectra of points D, E, and F marked in Fig. 6 are checked by the QPmR routine for verification. Remarkably, these two SRB segments' destabilizing behaviors, namely, $\mathrm{RT}_{SRB} = +1$, are corroborated by the results shown in Fig. 7.

With the help of the method in [16], we conclude that the lumped control strategy Eqs. (2) in (40) never becomes stable for any values of τ_1, even if $\tau_1 = 0$. On the other hand, the stable strip in Fig. 6 illustrates a significant improvement of the delay robustness using the proposed distributed control strategy.

Finally, we are concerned with the computational efficiency of this example. We have the results shown in Table 3 by drawing the comparison between the two methods again. Notice that 76.75 GiB memory is used to calculate $D_{T_1}(\omega)$ when using the Sylvester-type method. In fact, the computational complexity grows rapidly as the dimension or the rank of the system matrices increases [34], implying that the calculations may crash when dealing with more

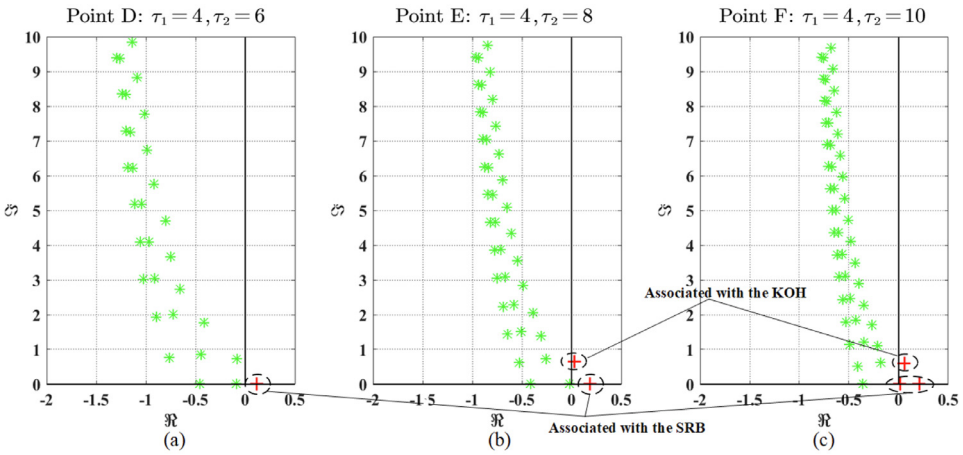

Fig. 7. Spectra of the original characteristic Eq. (4) for Case 2 using the QPmR routine (∗ - stable characteristic roots; + - unstable characteristic roots); (a) Point D with $\tau_1 = 4$, $\tau_2 = 6$; (b) Point E with $\tau_1 = 4$ and $\tau_2 = 8$; (c) Point F with $\tau_1 = 4$ and $\tau_2 = 10$.

Table 3
Comparisons of the time and memory usage between the Dixon-type resultant method and the Sylvester-type one for Case 2.

	Dixon-type resultant method	Sylvester-type resultant method
The first resultant step to obtain $R_{T_2}(\omega, T_1)$		
Dimensions of the matrix	$\mathbf{F}_1 : 3 \times 3$	$\mathbf{S}_1 : 6 \times 6$
Memory used	9.52 KiB	1320.96 KiB
CPU time	0 ns	16000000 ns
The second resultant step to obtain $D_{T_1}(\omega)$		
Dimensions of the matrix	$\mathbf{F}_2 : 18 \times 18$	$\mathbf{S}_2 : 35 \times 35$
Memory used	12.70 GiB	76.75 GiB
CPU time	130.80 s	738.00 s

complicated cases, e.g., $n = 8$ or $\text{rank}(\mathbf{B}) = 4$. However, our Dixon-type method has more room for such cases.

5. Conclusion

The stability problem of a general class of LTI distributed delay systems with the constant-coefficient, partial delay distribution is studied. To the best of our knowledge, it is the first attempt to treat this control scheme as an effective approach to enhance the system's delay robustness. For this, we provide a comprehensive stability analysis of the system, which necessitates the PSCC in the domain of delays. First, we present the equivalent system Eq. (9) with two lumped delays for the ease of the stability assessment. Second, we deal with the associated standing root case to determine what we call the SRB. Third, the Dixon resultant theory is proposed to obtain the exact bounds of the imaginary spectra. With this frequency range, we obtain the KOH by the frequency sweeping technique. We then utilize the CTCR paradigm to reveal the stability map for the systems of interest, which is verified by both the QPmR routine and the Simulink-based simulation. Additionally, we compare our proposed Dixon-

type resultant method to the Sylvester-type one to indicate its superiority in the computational efficiency. Future work includes the extension of the proposed procedure for the system with multiple distributed delays and the detailed theoretical analysis concerning the computational efficiency of the Dixon-type resultant method.

Declaration of Competing Interest

The authors declare that they have no known competing financial interests or personal relationships that could have appeared to influence the work reported in this paper.

Acknowledgment

This work is supported by Shenzhen excellent scientific and technological innovation talent training project under grant RCJC20200714114436040.

Appendix. Review of the CTCR paradigm [17]

The CTCR paradigm, an effective stability analysis tool for the LTI time-delay systems with p independent constant delays, determines the so-called "clustering features" of the infinitely many delay compositions corresponding to the imaginary roots of the system. Then, the analysis is reduced to be computationally manageable. In what follows, we present some key definitions and propositions of the CTCR paradigm by denoting the characteristic equation as $f(s, \boldsymbol{\tau}) = 0$.

Definition 3 (. *Kernel Hypersurfaces (KH)*) The kernel hypersurfaces are defined in the parameter space of $\boldsymbol{\tau} \in \mathbb{R}^{p+}$ as

$$\mathrm{KH} = \left\{\boldsymbol{\tau} \in \mathbb{R}^{p+} | f(s = \omega i, \boldsymbol{\tau}) = 0, 0 < \tau_k \omega < 2\pi, k = 1, 2, \ldots, p\right\}. \tag{42}$$

Definition 4 (. *Offspring Hypersurfaces (OH)*) The offspring hypersurfaces are defined by the following pointwise nonlinear transformation of the KH,

$$\left\langle \left\{ \tau_1 \pm \frac{2\pi}{\omega} l_1, \tau_2 \pm \frac{2\pi}{\omega} l_2, \ldots, \tau_p \pm \frac{2\pi}{\omega} l_p \right\} \right\rangle, l_k = 1, 2, \ldots, k = 1, 2, \ldots, p. \tag{43}$$

Moreover, the union of the KH and OH is defined as the KOH.

Definition 5 (. *Root Tendency (RT)*) The root tendency is defined to evaluate the transitional direction of the purely imaginary roots as

$$\mathrm{RT}|_{s=\omega i}^{\tau_k} = \mathrm{sgn}\left[\Re\mathfrak{e}\left(\frac{\partial s}{\partial \tau_k}\bigg|_{s=\omega i} \right) \right]. \tag{44}$$

where only one of the delays, i.e., τ_k, is increased by ε, $0 < \varepsilon \ll 1$, while all the other delays are fixed.

Obviously, $\mathrm{RT} = +1$ indicates a destabilizing crossing at the imaginary axis. Correspondingly, $\mathrm{RT} = -1$ implies the opposite behavior.

Proposition 1 (Finite number property [17])**.** *The number of the KH segments is upper bounded by the square of the order of the LTI delayed system.*

Proposition 2 (Invariant property [18])**.** *The root tendency has the property of remaining invariant from a given point on the KH to its corresponding mapping points on the OH when varying only one delay and keeping the others fixed.*

References

[1] X.-G. Li, S.-I. Niculescu, A. Çela, L. Zhang, Stability analysis of uniformly distributed delay systems: a frequency-sweeping approach, in: Delays and Interconnections: Methodology, Algorithms and Applications, Springer, Cham, 2019, pp. 117–130.

[2] R. Sipahi, F.M. Atay, S.-I. Niculescu, Stability of traffic flow behavior with distributed delays modeling the memory effects of the drivers, SIAM J. Appl. Math. 68 (3) (2008) 738–759, doi:10.1137/060673813.

[3] Y.-J. Chen, X.-G. Li, Y. Zhang, S.-I. Niculescu, A. Çela, Stability analysis of car-following systems with uniformly distributed delays using frequency-sweeping approach, IEEE Access 9 (2021) 69747–69755, doi:10.1109/ACCESS.2021.3077513.

[4] Y. Cao, Bifurcations in an internet congestion control system with distributed delay, Appl. Math. Comput. 347 (2019) 54–63, doi:10.1016/j.amc.2018.10.093.

[5] N. Olgac, A.S. Kammer, Stabilisation of open-loop unstable plants under feedback control with distributed delays, IET Control Theory Appl. 8 (10) (2014) 813–820, doi:10.1049/iet-cta.2013.0652.

[6] L. Zhang, Z.-Z. Mao, X.-G. Li, S.-I. Niculescu, A. Çela, Stability analysis for a class of distributed delay systems with constant coefficients by using a frequency-sweeping approach, IET Control Theory Appl. 13 (1) (2019) 87–95, doi:10.1049/iet-cta.2018.5520.

[7] D. Pilbauer, W. Michiels, T. Vyhlídal, Distributed delay input shaper design by optimizing smooth kernel functions, J. Franklin Inst. 354 (13) (2017) 5463–5485, doi:10.1016/j.jfranklin.2017.06.002.

[8] D. Pilbauer, T. Vyhlídal, W. Michiels, Optimized design of robust resonator with distributed time-delay, J. Sound Vib. 443 (2019) 576–590, doi:10.1016/j.jsv.2018.12.002.

[9] Q. Gao, N. Olgac, Optimal sign inverting control for time-delayed systems, a concept study with experiments, Int. J. Control 88 (1) (2015) 113–122, doi:10.1080/00207179.2014.941409.

[10] C.-K. Zhang, F. Long, Y. He, W. Yao, L. Jiang, M. Wu, A relaxed quadratic function negative-determination lemma and its application to time-delay systems, Automatica 113 (2020) 108764, doi:10.1016/j.automatica.2019.108764.

[11] Z. Feng, H. Zhang, H.-K. Lam, New results on dissipative control for a class of singular Takagi-Sugeno fuzzy systems with time delay, IEEE Trans. Fuzzy Syst. (Early Access) (2021), doi:10.1109/TFUZZ.2021.3086227.

[12] R. Sipahi, I.I. Delice, Advanced clustering with frequency sweeping methodology for the stability analysis of multiple time-delay systems, IEEE Trans. Automat. Control 56 (2) (2011) 467–472, doi:10.1109/TAC.2010.2090734.

[13] Q. Gao, A.S. Kammer, U. Zalluhoglu, N. Olgac, Combination of sign inverting and delay scheduling control concepts for multiple-delay dynamics, Syst. Control Lett. 77 (2015) 55–62, doi:10.1016/j.sysconle.2015.01.001.

[14] X.-G. Li, S.-I. Niculescu, A. Çela, L. Zhang, X. Li, A frequency-sweeping framework for stability analysis of time-delay systems, IEEE Trans. Automat. Control 62 (8) (2017) 3701–3716, doi:10.1109/TAC.2016.2633533.

[15] L. Pekař, Q. Gao, Spectrum analysis of LTI continuous-time systems with constant delays: a literature overview of some recent results, IEEE Access 6 (2018) 35457–35491, doi:10.1109/ACCESS.2018.2851453.

[16] N. Olgac, R. Sipahi, An exact method for the stability analysis of time-delayed linear time-invariant (LTI) systems, IEEE Trans. Automat. Control 47 (5) (2002) 793–797, doi:10.1109/TAC.2002.1000275.

[17] A.F. Ergenc, N. Olgac, H. Fazelinia, Extended Kronecker summation for cluster treatment of LTI systems with multiple delays, SIAM J. Control Optim. 46 (1) (2007) 143–155, doi:10.1137/06065180X.

[18] R. Sipahi, N. Olgac, Complete stability robustness of third-order LTI multiple time-delay systems, Automatica 41 (8) (2005) 1413–1422, doi:10.1016/j.automatica.2005.03.022.

[19] J. Chen, H.A. Latchman, Frequency sweeping tests for stability independent of delay, IEEE Trans. Automat. Control 40 (9) (1995) 1640–1645, doi:10.1109/9.412637.

[20] Q. Gao, N. Olgac, Bounds of imaginary spectra of LTI systems in the domain of two of the multiple time delays, Automatica 72 (2016) 235–241, doi:10.1016/j.automatica.2016.05.011.

[21] O. Toker, H. Özbay, Complexity issues in robust stability of linear delay-differential systems, Math. Control Signals Syst. 9 (1996) 386–400, doi:10.1007/BF01211858.

[22] M.A. Pakzad, Stability analysis of LTI fractional-order systems with distributed delay, in: 2021 60th IEEE Conference on Decision and Control (CDC), IEEE, 2021, pp. 5484–5489, doi:10.1109/CDC45484.2021.9683617.

[23] C. Yuan, S. Song, Q. Gao, H.R. Karimi, L. Pekar, S. Guo, A novel frequency-domain approach for the exact range of imaginary spectra and the stability analysis of LTI systems with two delays, IEEE Access 8 (2020) 36595–36601, doi:10.1109/ACCESS.2020.2973834.

[24] H. Fazelinia, R. Sipahi, N. Olgac, Stability robustness analysis of multiple time-delayed systems using "building block" concept, IEEE Trans. Automat. Control 52 (5) (2007) 799–810, doi:10.1109/TAC.2007.898076.

[25] R. Courant, Differential and Integral Calculus, Wiley Interscience, London, 1988.

[26] R. Jenkins, N. Olgac, New perspectives on criticality of multiple identical imaginary roots (MIR) in time-delayed systems, in: 2018 Annual American Control Conference (ACC), IEEE, 2018, pp. 2845–2850, doi:10.23919/ACC.2018.8431005.

[27] A.L. Dixon, The eliminant of three quantics in two independent variables, in: Proceedings of the London Mathematical Society, vol. 2, Narnia, 1909, pp. 49–69, doi:10.1112/plms/s2-7.1.49.

[28] D. Kapur, T. Saxena, Comparison of various multivariate resultant formulations, in: 1995 International Symposium on Symbolic and Algebraic Computation, Association for Computing Machinery, 1995, pp. 187–194, doi:10.1145/220346.220370.

[29] G. Lou, W. Gu, Y. Xu, W. Jin, X. Du, Stability robustness for secondary voltage control in autonomous microgrids with consideration of communication delays, IEEE Trans. Power Syst. 33 (4) (2018) 4164–4178, doi:10.1109/TPWRS.2017.2782243.

[30] A. Ramírez, R. Sipahi, Multiple intentional delays can facilitate fast consensus and noise reduction in a multi-agent system, IEEE Trans. Cybern 49 (4) (2019) 1224–1235, doi:10.1109/TCYB.2018.2798163.

[31] J. Cai, X. Zhang, Q. Gao, Exact stability analysis of LTI systems with multiple distributed delays based on the Dixon resultant, in: 2021 40th Chinese Control Conference (CCC), IEEE, 2021, pp. 994–999, doi:10.23919/CCC52363.2021.9550018.

[32] R. Sipahi, S.-I. Niculescu, Slow time-varying delay effects-robust stability characterization of deterministic car following models, in: IEEE International Conference on Computer-Aided Design, IEEE, 2006, pp. 2219–2224, doi:10.1109/CACSD-CCA-ISIC.2006.4776985.

[33] T. Vyhlidal, P. Zítek, Mapping based algorithm for large-scale computation of quasi-polynomial zeros, IEEE Trans. Automat. Control 54 (1) (2009) 171–177, doi:10.1109/TAC.2008.2008345.

[34] R. Sipahi, N. Olgac, Stability robustness of retarded LTI systems with single delay and exhaustive determination of their imaginary spectra, SIAM J. Control Optim. 45 (5) (2006) 1680–1696, doi:10.1137/050633238.